Where can we find a seasonal cycle of the Atlantic water temperature within the Arctic Basin?

Camille Lique, Michael Steele

Where can we find a seasonal cycle of the Atlantic water temperature within the Arctic Basin?

Camille Lique[1] and Michael Steele[2]

Received 20 September 2011; revised 5 January 2012; accepted 27 January 2012; published 17 March 2012.

[1] Recent mooring observations in the Arctic Basin suggest the existence of a seasonality of Atlantic Water (AW) temperature. Here the DRAKKAR global ocean/sea-ice model is used to examine the seasonal cycle amplitude of AW temperature within the Arctic Ocean and to investigate the possible mechanisms governing this seasonality. The simulation as well as available mooring data reveals that the amplitude of the AW temperature seasonal cycle is significant only in the Nansen Basin along the continental slope, where AW is primarily advected. In the model, the seasonal cycle of the AW temperature is advected from Fram Strait up to St. Anna Trough and then re-energized by the Barents Sea Branch. This suggests that the seasonal AW temperature signal survives over a finite distance (∼1000 km). Interannual changes in the seasonal cycle amplitude can be as large as the mean seasonal cycle amplitude; thus seasonality is difficult to characterize from observations spanning only a short period. The seasonal bias of in-situ observations taken during spring and summer does not induce a large error when considering the interannual-to-decadal variations of AW temperature, because the seasonal cycle accounts for a small or negligible part of AW temperature variability, even near the inflow region.

Citation: Lique, C., and M. Steele (2012), Where can we find a seasonal cycle of the Atlantic water temperature within the Arctic Basin?, *J. Geophys. Res.*, *117*, C03026, doi:10.1029/2011JC007612.

1. Introduction

[2] Warm (T ∼ 2–3°C) and relatively salty (S ∼ 35 psu) water is advected from the North Atlantic to the Arctic Ocean through Fram Strait and the Barents Sea, and plays a crucial role for the thermal balance of the Arctic Ocean. As it penetrates the Arctic Basin, Atlantic Water (AW) descends beneath the fresher, colder mixed layer in the Nansen Basin. AW circulates cyclonically around the Eurasian and Canadian Basins, primarily following the topography [e.g., *Coachman and Barnes*, 1963; *Rudels et al.*, 1994, 1999; *Schauer et al.*, 2002b; *Nøst and Isachsen*, 2003; *Aksenov et al.*, 2011]. During its transit along the Arctic slope, AW undergoes freshening and large cooling [*Karcher and Oberhuber*, 2002; *Lique et al.*, 2010], and is eventually exported to the North Atlantic.

[3] Because AW is considerably warmer than surface and bottom water masses (Figure 1), the distribution of its maximum temperature is often used to follow the circulation and transformations of the AW layer [*Coachman and Barnes*, 1963; *Karcher et al.*, 2003]. Figure 2 shows a map of the mean maximum temperatures. Herein, the maximum temperature detected for each temperature profile and for salinity greater than 34.7 is called Atlantic Water core temperature (AWCT). This salinity limit is found to be suitable to detect AW in the Barents Sea [*Smolyar and Adrov*, 2003].

[4] Substantial variability and changes affecting the AW properties over the past decades have been reported in the literature. Increases in the transport volume and the temperature of AW inflow through Fram Strait [*Schauer et al.*, 2002a] or the Barents Sea route [*Furevik*, 2001; *Karcher et al.*, 2003] are responsible for strong warming events in the AW layer observed within the Nansen and Canadian basins [*Quadfasel et al.*, 1991; *Carmack et al.*, 1997; *Polyakov et al.*, 2004, 2005; *Dmitrenko et al.*, 2008; *McLaughlin et al.*, 2009]. *Polyakov et al.* [2004] suggest that AW temperature variations might be dominated by low-frequency oscillations over a 50–80 year timescale.

[5] In these observational studies, researchers often compare hydrographic data from different time periods, without regard to the season when the measurements were conducted. For instance, *Polyakov et al.* [2004] average all hydrographic data available since 1900 within 10 spatial boxes year by year. This strategy may be justified because the water masses examined here lie at intermediate depths (deeper than 200 m; Figure 1), so that the mixed layer and cold halocline above prevent AW from contact with the atmosphere, which is the primary source of the seasonal temperature variations in the global ocean [e.g., *Yashayaev and Zveryaev*, 2001].

[6] Although rarely taken into account, evidence of an AW temperature seasonality has been highlighted recently from mooring observations around the Nansen Basin, but the origin of this seasonality remains subject to discussion. *Ivanov*

[1]Joint Institute for the Study of the Atmosphere and Ocean, University of Washington, Seattle, Washington, USA.
[2]Polar Science Center, Applied Physics Laboratory, University of Washington, Seattle, Washington, USA.

0148-0227/12/2011JC007612

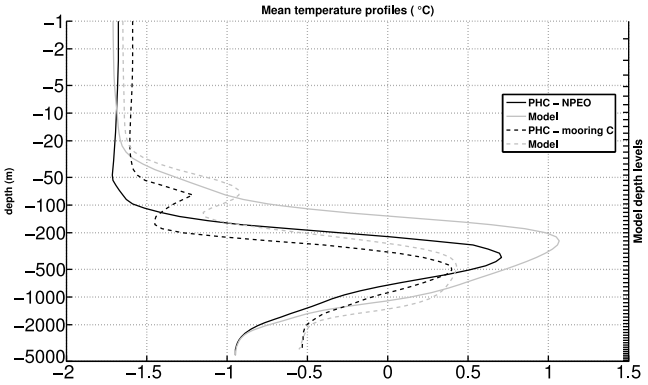

Figure 1. Mean temperature profiles in the Eurasian Basin (at the NPEO mooring, solid line) and in the Canadian Basin (at the BGOS-C mooring, dashed line) for the simulation (black) and the PHC climatology (gray). Note that the vertical scale is logarithmic. The model depth levels are shown on the right-hand vertical scale. See Figure 3 for the location of the moorings.

et al. [2009] report a seasonal cycle of the AWCT north of Spitsbergen at 31°E (mooring M3, see Figure 3) with a peak-to-peak amplitude of 1.2°C over 2005–2006. They suggest that the seasonal cycle might be advected from Fram Strait, where a strong seasonal cycle is well documented [*Schauer et al.*, 2002a]. Further downstream, *Dmitrenko et al.* [2006] also report on a seasonal cycle at the southern Laptev Sea over 2002–2004 (mooring M1, see Figure 3), but they attribute this seasonality to a shift of the AW core toward the slope in winter and away in summer, possibly due to seasonal local wind variations. Their conclusions about the AW core shift, however, are based on observations from only one mooring, which makes it impossible to detect spatial variations. *Dmitrenko et al.* [2009], also using mooring data downstream in the Laptev Sea (mooring M2, see Figure 3), report on a seasonal cycle of the temperature at 260 m with a peak-to-peak amplitude of 0.25°C over 2004–2007, and suggest that the seasonality is primarily translated from Fram Strait. They also speculate that the seasonality of the AWCT could be affected by the interactions between the Fram Strait and the Barents Sea branches. At the same time, year-long mooring data (1995–1996) from the eastern Laptev Sea do not show evidence of seasonality [*Woodgate et al.*, 2001].

[7] Although these studies suggest a large temperature seasonality within the AW layer, the observations used in these studies are too sparse in time and space to allow a description of AW temperature seasonality on an Arctic Basin scale. Here, we use output from a global ocean/sea ice coupled model to map the seasonal cycle amplitude of the AWCT in the Arctic Basin. The simulation also allows an examination of the interannual changes in the seasonal cycle amplitude, and to understand the processes responsible for this seasonality. The model simulation also provides insight on possible errors induced by the spring-summer seasonal observation bias used to study the long-term variations of AW temperature in the Arctic Basin.

[8] This paper is organized as follows. The model and experimental design are described briefly in Section 2. In Section 3, the simulation realism is assessed, comparing it with available mooring data from different locations in the Arctic Basin. Mean and interannual changes of the AWCT seasonal cycle amplitude are described in Section 4, while the mechanisms at play for this seasonality are investigated in Section 5. The possible implications of seasonal AW temperature cycle on observational studies of AW temperature temporal variations and trends are discussed in Section 6.

2. Numerical Experiment Description and Design

[9] The global ORCA025 coupled ocean/sea-ice model configuration developed by the DRAKKAR project [*The DRAKKAR Group*, 2007] is used to perform the simulation.

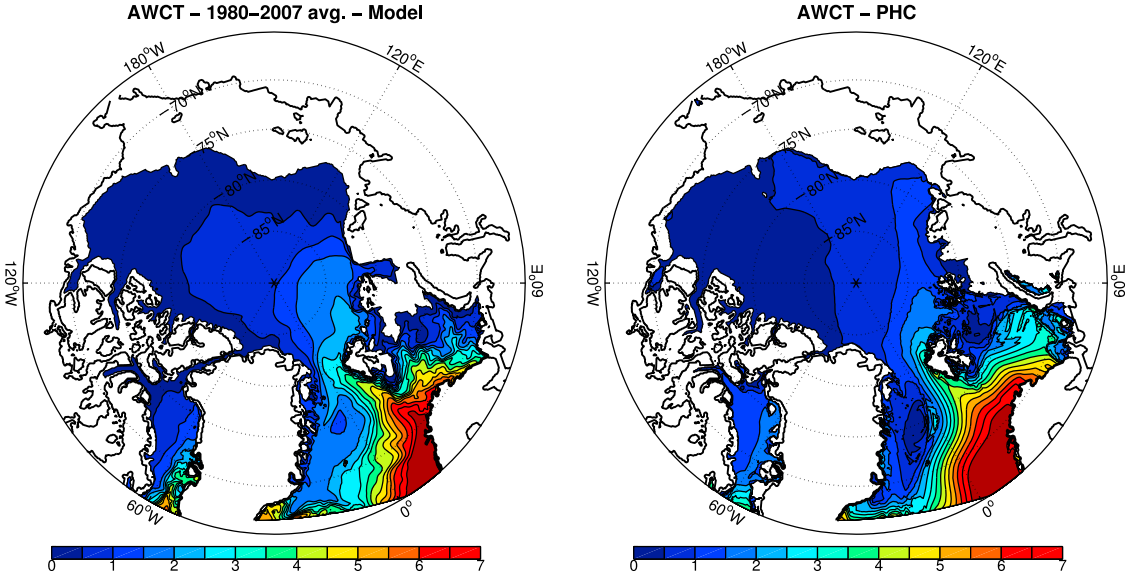

Figure 2. Mean AWCT distribution computed from (left) the simulation and (right) the PHC climatology. Note that a determination of AWCT is only made for AW with salinity greater than 34. AWCT shallower than 200 m and colder than 0°C are not displayed.

Figure 3. Location of the moorings and sections used in the text. Bathymetry contours 500, 1000, 1500, 2000, 3000, 4000 and 5000 m are drawn with a thin line. The 1500 m isobath used in Section 5 is also shown (dashed line). Circles indicate the NPEO mooring, pluses indicate the NABOS moorings and crosses indicate the BGOS moorings.

An overall description of the model and its numerical details is given by *Barnier et al.* [2006]. This model configuration uses a global tripolar grid with 1442 × 1021 grid points and 75 vertical levels. Vertical grid spacing is finer near the surface (1 m) and increases with depth to 200 m at the bottom. Horizontal resolution is 27.75 km at the equator, 13.8 km at 60°N, and gets to 10 km in the Arctic Ocean. The ocean/sea-ice code is based on the NEMO (Nucleus for European Modelling of the Ocean) framework version 3.1 [*Madec*, 2008]. It uses a partial step representation of the bottom topography and an energy-enstrophy conserving momentum advection scheme [*Penduff et al.*, 2007]. Parameterizations include a Laplacian mixing of temperature and salinity along isopycnals, a horizontal biharmonic viscosity, and a turbulence closure scheme (TKE) for vertical mixing. A parametrization of the solar vertical penetration modulation by the phytoplankton concentration (using a monthly climatology of the sea surface color derived from SeawiFS satellite observations) has also been added because it improves the representation of the sea ice conditions [*Lengaigne et al.*, 2009]. The bathymetry is derived from the 1-minute resolution Etopo1 bathymetry file of NGDC (National Geophysical Data Center). The sea-ice model is the Louvain-la-Neuve model, which is a dynamic-thermodynamic model specifically designed for climate studies. A detailed description is given by *Timmermann et al.* [2005].

[10] Our experiment runs from 1958 to 2007 with no spin-up. Initialization uses January data from the Polar Science Center Hydrographic T/S Climatology (PHC; see *Steele et al.* [2001] for details). The forcing data set is a blend of data from various origins at different frequencies [*Brodeau et al.*, 2010]. Precipitation and radiation are from the CORE data set [*Large and Yeager*, 2004] at monthly and daily frequency, respectively, based on satellite observations when available. A climatology of the same satellite data set is used for the early years up to 1979 and 1984, respectively. Air temperature, humidity, and wind speed are six-hourly fields from the ECMWF reanalysis ERA40 (1958–2001) and the ECMWF Operational Analysis (2002–2007). Turbulent fluxes (wind stress, latent and sensible heat flux) are estimated using the CORE bulk formulae [*Large and Yeager*, 2004]. River runoff rates are prescribed using the *Dai and Trenberth* [2002] climatological data set. To avoid an excessive model drift, a relaxation of sea surface salinity is added to the PHC climatology. The coefficient (0.027 m/day) amounts to a decay time of 371 days for 10 m of water depth; under the ice cover restoring is five times stronger. The analysis presented here focuses on a 27-year period from 1980 to 2007, excluding the early years of the simulation to allow for model adjustment.

3. Observed and Model Simulated AW Temperature Seasonal Cycles at Mooring Locations

[11] A similar setup of the model has been used previously for studies of Arctic oceanography, and extended evaluation of the ocean and sea ice model components is given by *Lique et al.* [2009, 2010]. Figure 2 compares the mean AWCT (the average over 1980–2007) and the PHC climatology [*Steele et al.*, 2001]. A similar figure is given for instance by *Dmitrenko et al.* [2008] (using historical data over 1894–1990) and *Karcher et al.* [2003] (computed from their model outputs). The model and the climatology both show warm water at the surface entering the Arctic Ocean via Fram Strait and the Barents Sea. North of Spitsbergen, AW descends to 200–300 m as it penetrates the Nansen Basin (not shown). Compared to PHC, the modeled distribution of AWCT does not show a clear front that would correspond to the Lomonosov Ridge. In contrast, the model exhibits a larger recirculation that starts north of the St. Anna Trough. This is a common feature among Arctic models, possibly due to a misrepresentation of the eddy activity or flaws in the mixing parameterizations [*Hunke et al.*, 2008]. As a consequence, the mean modeled AWCT at the southern Laptev Sea is about 1°C too cold compared to the climatology or to the results reported by *Dmitrenko et al.* [2008]. Note that the modeled AWCT is a bit warmer than the PHC climatology at the NPEO and BGOS-C mooring locations (Figure 1), but the difference could be explained by the fact that the climatology is heavily weighted toward the decades of the 1970s and 1980s when the Arctic Ocean was probably colder than the recent period [see, e.g., *Ivanov et al.*, 2009, Figure 3].

[12] Despite the mean AWCT cold bias, the basic features of the AWCT distribution are captured by the model simulation. In the following, we focus on the AW temperature seasonal variations, as we compare the model outputs against available observations from mooring at various locations within the Arctic Basin, as shown in Figure 3. The characteristics of the different moorings are summed up in Table 1. We also aim at taking advantage as best as we can of the available observations in order to get insight on the AWCT seasonal cycle amplitude at the Arctic Basin scale. For each mooring location, we determine the seasonal cycle amplitude (defined as the peak-to-peak amplitude in this study) and its timing of the AWCT (for profiling mooring) or the temperature at a depth

Table 1. Characteristics of the Different Moorings Used in This Study

Name	Instrument Type	Location and Depth	Time Period	Data Source
Fram Strait Section	between 11 and 17 moorings, depending on the year	78°50′N between 5°E and 8°40′E, from the surface to 700 m	1997–2004	See http://www.whoi.edu/page.do?pid=30914. Time series of monthly means were provided.
Kola Section	CTD casts taken several times each year	33°30′E between 70°30′N and 72°30′N, from the surface to 200 m	1950–2011	Provided by PINRO, Murmansk, Russia. Time series of monthly means were provided.
NABOS M1	1 m resolution profiling mooring	78°26′N, 125°35′E, profiles from the surface to 2500 m	2002–2006	See http://nabos.iarc.uaf.edu/index.php. Profiles span from 150 to 2000 m. Note that we have first binned the data into the model layers before detecting the maximum T.
NABOS M2	discrete fixed-depth CTDs on a mooring	79°55′N, 142°21′E, close to 270 m	2004–2007	The depth of the instrument varies each year: 253 m and 297 m (2004–2005), 275 m (2005–2006) and 280 m (2006–2007).
NABOS M3	discrete fixed-depth CTDs on a mooring	81°30′N, 31°E, at 215 m	2004–2007	
NPEO	discrete fixed-depth CTDs on a mooring	50–80 km from the North Pole, at 260 m	2001–2010	See http://psc.apl.washington.edu/northpole/.
BG A	1 m resolution profiling mooring	75°N, 149°58′W	2003–2009	See http://www.whoi.edu/beaufortgyre/. Profiles span from 150 to 2000 m. Note that we have first binned the data into the model layers before detecting the maximum T.
BG B	1 m resolution profiling mooring	78°N, 150°4′W	2003–2009	
BG C	1 m resolution profiling mooring	76°59′N, 139°57′W	2003–2009	
BG D	1 m resolution profiling mooring	74°N, 140°W	2005–2009	

close the AW core (for fixed-depth instruments). Although the observed time series are often short (a few years), we also compute when possible a Fourier analysis of the temperature time series, in order to get an idea of the importance of the annual harmonic compared to other frequencies.

3.1. AW Inflow

[13] Intensive monitoring of AW inflow to the Arctic Basin through Fram Strait [e.g., *Schauer et al.*, 2004] and the Barents Sea [e.g., *Loeng*, 1991] has been conducted over the past decades. Figure 4 shows the model simulated temperature through Fram Strait and the Kola section, compared with observations from the mooring array through Fram Strait at 78°50′N and in situ measurements through the Kola section. Across these sections, AW extends from the surface to the bottom, and is thus in contact with the atmosphere and its seasonal temperature cycle. The AWCT is found at the surface in summer, and near 200 m in winter. Temperature observations through the east side of Fram Strait show a large seasonal cycle over 1998–2004, with an amplitude varying between 1 and 2°C, and a maximum occurring in late summer (October) and a minimum in March. A harmonic analysis reveals that the annual harmonic accounts for the bulk part of the temperature variance (56%). The simulation reproduces fairly well the AW temperature seasonal cycle, although its amplitude is generally smaller (between 0.7 and 1.3°C) than the observations.

[14] Along the Kola section, the model simulated temperature presents a 1°C cold bias, which might be due to a problem of the simulated AW pathway within the Barents Sea as the Kola section samples only a limited part of the AW Barents Sea branch. The mean temperature from the surface to 200 m exhibits a large seasonal cycle that accounts for 60% of the variance. The timing is similar to that in Fram Strait, but the amplitude is larger (between 1.6 and 3°C). This amplitude difference might be due to both the location of the section further south and the shallower depths considered here, the water column being warmer close to the surface.

3.2. Eurasian Basin

[15] After entering the Arctic Basin through Fram Strait and St. Anna Trough in the northern Barents Sea, AW circulates cyclonically along the slope of the Eurasian Basin [*Schauer et al.*, 2002b]. Several moorings have been deployed since the 2000s around the Eurasian Basin as part of the NABOS (Nansen and Amundsen Basins Observational System) [*Polyakov et al.*, 2003] and NPEO (North Pole Environmental Observatory) [*Morison et al.*, 2002]. Figure 5 shows the monthly mean temperature variations computed from four different moorings, compared to the model temperature variations at the same locations.

[16] We examine the variations of temperature northeast of Fram Strait at mooring M3 at about 215 m depth, which is close to the depth of the AWCT [*Ivanov et al.*, 2009]. Using two years of observations (2004–2006), *Ivanov et al.* [2009] report that the annual harmonic from a harmonic analysis has an amplitude between 0.9 and 1.3°C, with a maximum and a minimum occurring in November and May, respectively, i.e one to two months later than in Fram Strait. The annual harmonic accounts for 25% of the observed time series variance over 2004–2009 and the amplitude reduces to 0.36°C over this longer period. The model simulated seasonal cycle of the temperature at 215 m depth at M3 over the

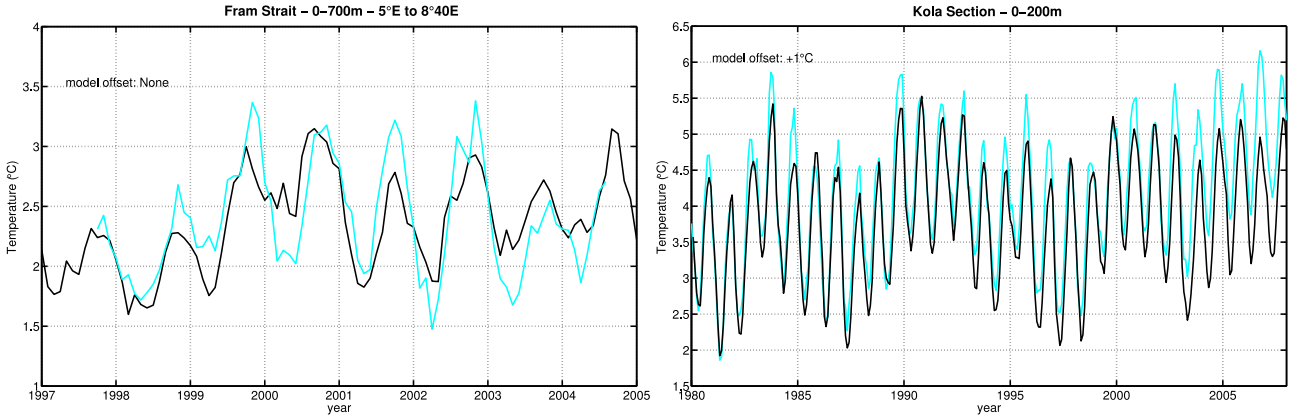

Figure 4. (left) Monthly model simulated (black) and observed (cyan) mean temperature averaged through Fram Strait (at 78°50′N between 5°E and 8°40′E) from the surface to 700 m. No offset has been added to the model time series. (right) Monthly model simulated (black) and observed (cyan) mean temperature averaged through the Kola section (at 33°30′E between 70°30′N and 72°30′N) from the surface to 200 m. Note that a +1 °C offset has been added to the model temperature time series.

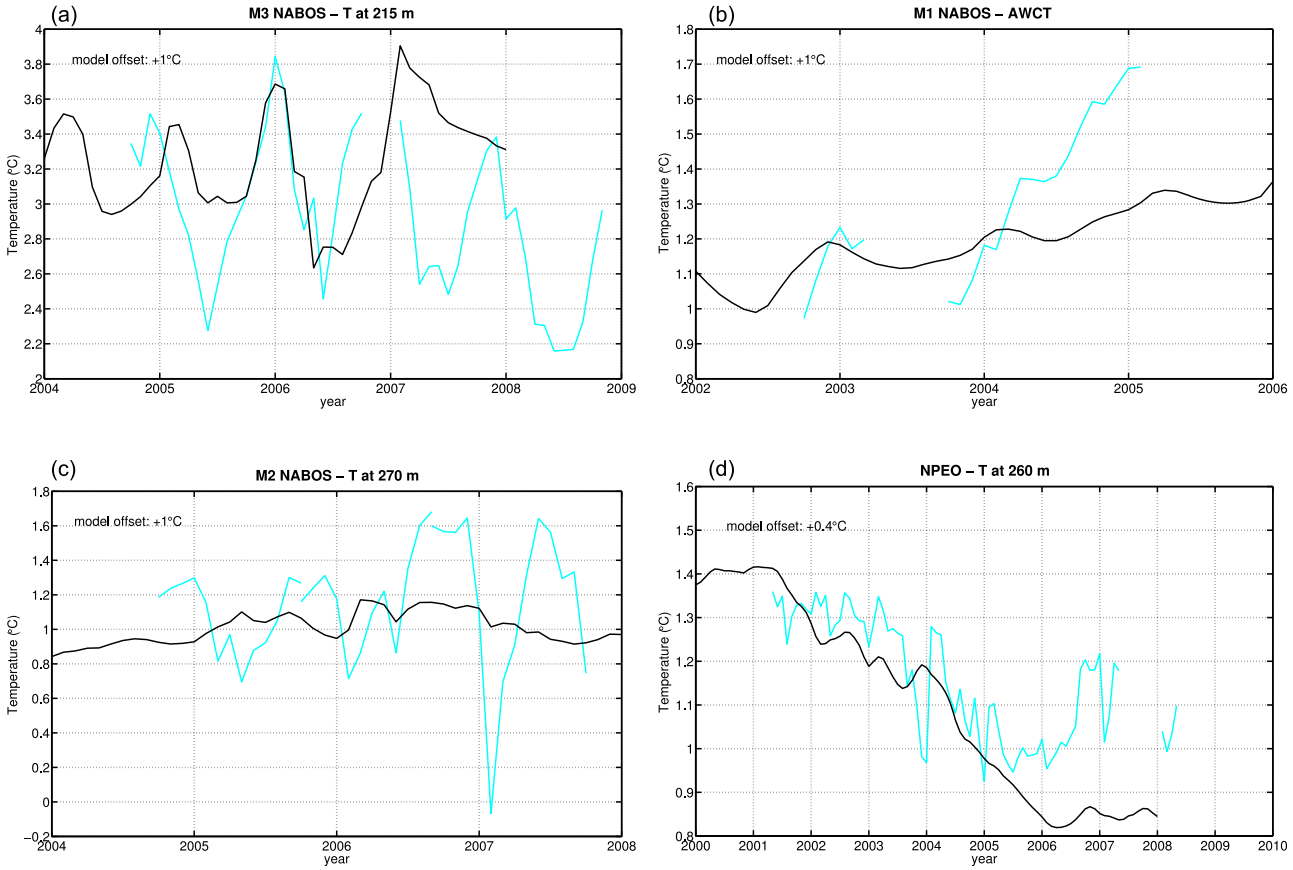

Figure 5. (a) Monthly mean temperature at the NABOS M3 mooring at 215 m. (b) Monthly mean AWCT at the NABOS M1 profiling mooring. (c) Monthly mean temperature at the NABOS M2 mooring at about 270 m. The discontinuity for the observations is due to small changes of instrument depth (see Table 1). (d) Monthly mean temperature at the NPEO mooring at 250 m. The simulated (black) and observed (cyan) temperatures are shown. Note that a +1°C offset and a +0.4°C offset have been added to the model temperature time series for the NABOS and NPEO mooring, respectively. See Figure 3 for the location of the moorings.

last five years of the simulation (2002–2007) underestimates the amplitude of the seasonal cycle (0.21°C in the model), though the variances explained by the modeled and observed seasonal cycle are similar. Both the model results and the longer observational time series also reveal that the amplitude and timing of the seasonal cycle vary from year to year.

[17] Downstream from M3, a profiling mooring (M1) was deployed north of the Laptev Sea over 2002–2006 [*Dmitrenko et al.*, 2006, 2008]. Figure 5b shows the monthly mean AWCT computed from each profile of the profiling mooring. Using data from September to February in 2002 and 2003, *Dmitrenko et al.* [2006] find higher AW temperatures in winter than summer, and they attribute these variations to a seasonal cycle with an amplitude of about 0.2°C. After February 2004, the observed dominant signal is a large warming as discussed by *Dmitrenko et al.* [2008]. No evidence of a seasonality can be found when examining the entire observed time series (Figure 5b). The model fails at reproducing this large and sudden warming event after February 2004. However, the model simulated AWCT times series does exhibit a seasonal cycle with an amplitude of 0.1–0.2°C, and a warm season in fall-winter, in agreement with *Dmitrenko et al.* [2006], although the annual harmonic does not account for a significant part of the variance.

[18] At mooring M2 in the eastern Laptev Sea, the temperature time series over 2004–2007 exhibits a seasonal cycle amplitude of 0.25°C at 260 m (attributed to the Fram Strait Branch) and 0.05°C at 840 m (attributed to the Barents Sea Branch) [*Dmitrenko et al.*, 2009]. Figure 5c shows the model monthly mean temperature time series at 270 m at M2, and the mooring observations. Note that we are showing the time series from the closest instrument to the 270 m model depth level (see Table 1). The observed temperature time series exhibits a cold season followed by a warm season each year, although both the timing and the amplitude of the seasonal cycle are highly variable annually. The modeled temperature at 270 m time series does not exhibit a seasonal cycle. However, the modeled AWCT at M2 is deeper than 270 m, and varies annually around 500 m on the average. The model simulated AWCT variations at M2 (not shown) exhibit a seasonal cycle with an amplitude varying from 0.02°C to 0.15°C, depending on the year considered.

[19] At the eastern end of the Laptev Sea, the AW flow splits into two branches: one enters the Canadian Basin, while the second remains in the Amundsen Basin, flowing along the Lomonosov Ridge [*Rudels et al.*, 1999]. Since 2001, a mooring has been deployed and maintained close to the North Pole by the NPEO [*Aagaard et al.*, 2008]. The observed and modeled monthly mean temperature time series at 260 m depth show a general cooling trend and no seasonal cycle (Figure 5d). A harmonic analysis of the time series (not shown) suggests that the annual harmonic is very small at that location (both for the model and the observations over 2001–2008). There is no seasonality of the AWCT at the NPEO mooring location.

3.3. Canadian Basin

[20] Since August 2003, moorings have been deployed within the Canadian Basin as part of the Beaufort Gyre Observing System (BGOS) [*Proshutinsky et al.*, 2009]. The monthly mean observational time series of the AWCT at the four mooring locations compared with the model simulated time series at those locations shows an underestimation by the model of the variations of the maximum temperature (Figure 6; the observed variations have an amplitude of about 0.05°C). Neither the observations nor the model exhibit significant AWCT seasonality, according to a harmonic analysis of the modeled and observed AWCT time series.

[21] One could argue that these four moorings are in the Beaufort Gyre interior and might not be representative of what is happening along the slopes where AW is primarily advected [*Rudels et al.*, 1999]. We have thus also considered data from one mooring located on the 1600 m isobath of the Beaufort Sea slope north of Alaska (not shown) [see *Pickart et al.*, 2011]. A two-year time series of AWCT from this mooring's measurement also shows no evidence of a AWCT seasonal cycle at that location.

[22] In this section, we have tried to use all the mooring data available in the Arctic Basin to determine the spatial variations of the seasonal cycle amplitude of the AWCT. We therefore need observations over time periods longer than a year, and such observations are only available after 2000. This makes it difficult to distinguish between seasonal and other frequencies. However, clear evidence of a seasonality within the AW layer could be found, at least in the Nansen Basin, and its origin still needs to be investigated. Although our numerical simulation has a cold bias all over the Arctic Basin and might to some extent underestimate the amplitude of the AW temperature variations, it allows an examination of AWCT seasonality in a fully consistent way, taking advantage of the large coverage in time and space.

4. Model Simulated Amplitude of the AWCT Seasonal Cycle and Interannual Variability

[23] Our goal in this section is to provide an objective definition for the seasonal cycle amplitude of the AWCT, in order to describe it at the Arctic Basin scale, and to examine its variations over several decades. From now on, only results from the numerical simulation will be shown.

4.1. Definition of the Seasonal Cycle Amplitude: Example at the M3 Location

[24] In the previous section, we showed that the AWCT seasonal cycle amplitude might be highly variable at a given point depending on the year considered. We thus need as a first step to clearly define the quantities that we will examine.

[25] Figure 7 shows an example at one given point (M3) of the treatment that we apply to the AWCT time series to extract the amplitude and the phase of the seasonal cycle. First of all, we remove from the initial time series its running mean computed with a 12-month window, in order to obtain the seasonal AWCT time series. We then fit the annual harmonic to the seasonal AWCT time series, which yields the mean amplitude and the timing of the minimum and the maximum. The difference of amplitude and timing between the annual harmonic and the seasonal AWCT each year allows a quantification of the interannual variability of the seasonal cycle. The same treatment is applied at each model grid point over the period 1980–2007.

4.2. The Mean Seasonal Cycle Amplitude

[26] Figure 8 shows a map of the amplitude and phase of seasonal AWCT variations as well as the percent of the total

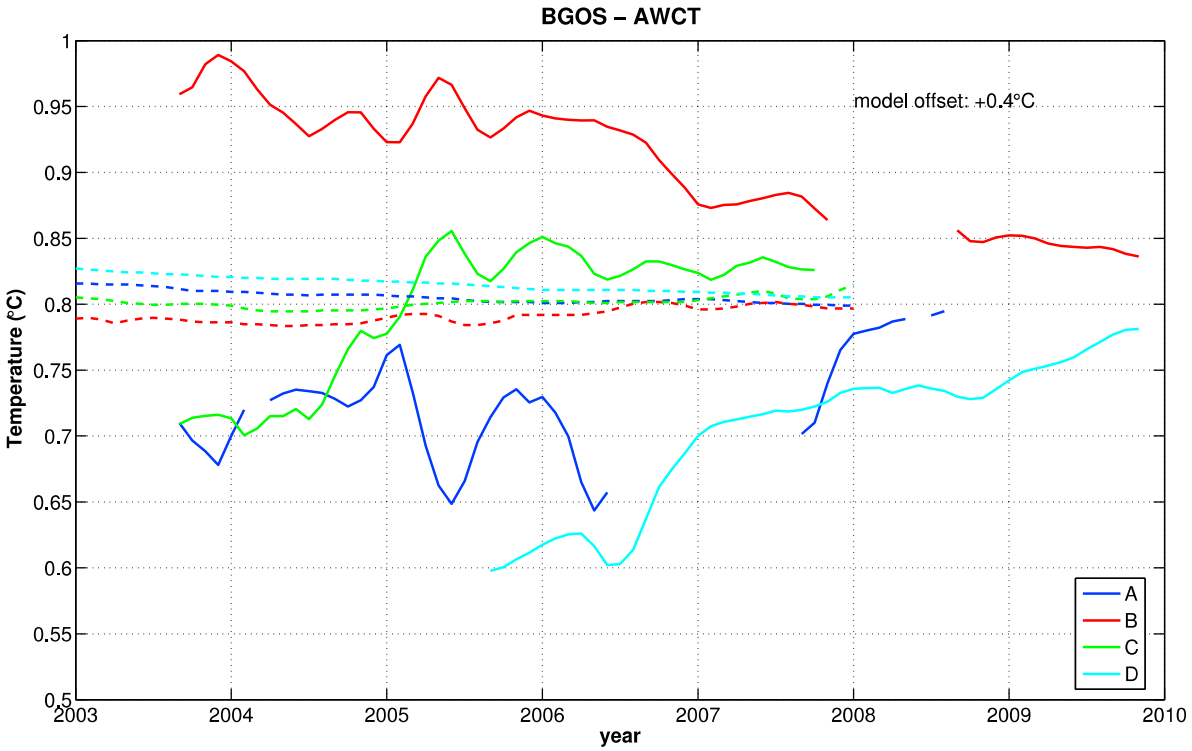

Figure 6. Monthly mean AWCT in the Beaufort Gyre at mooring locations (A, B, C and D; see Figure 3 for the location of the moorings). The simulated (dashed lines) and observed (solid lines) temperatures are shown. Note that a +0.4°C offset has been added to the model temperature time series.

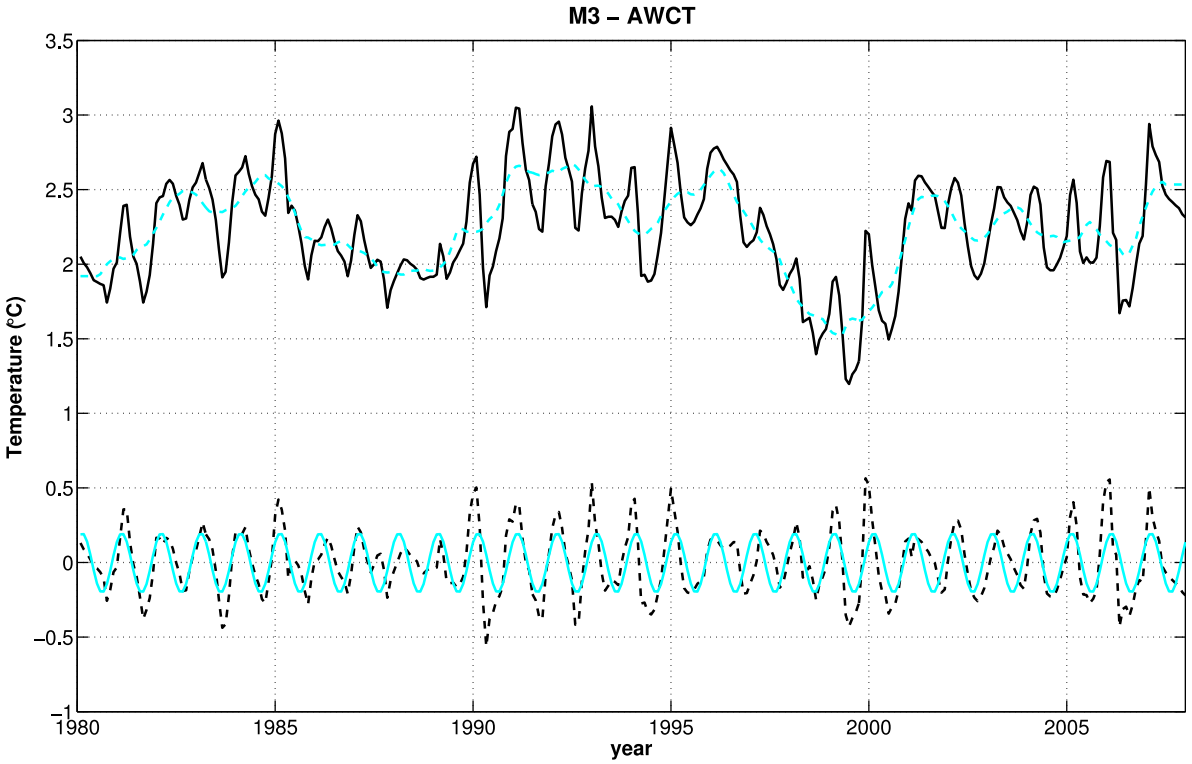

Figure 7. Definition of the seasonal cycle for the monthly mean AWCT at mooring M3 (see Figure 3 for the location of M3). The solid black line is the initial model time series, the dashed cyan line is the running mean of the time series with a 12-month window, the dashed black line is the result of the subtraction of the two previous time series, and the solid cyan line is the corresponding annual harmonic.

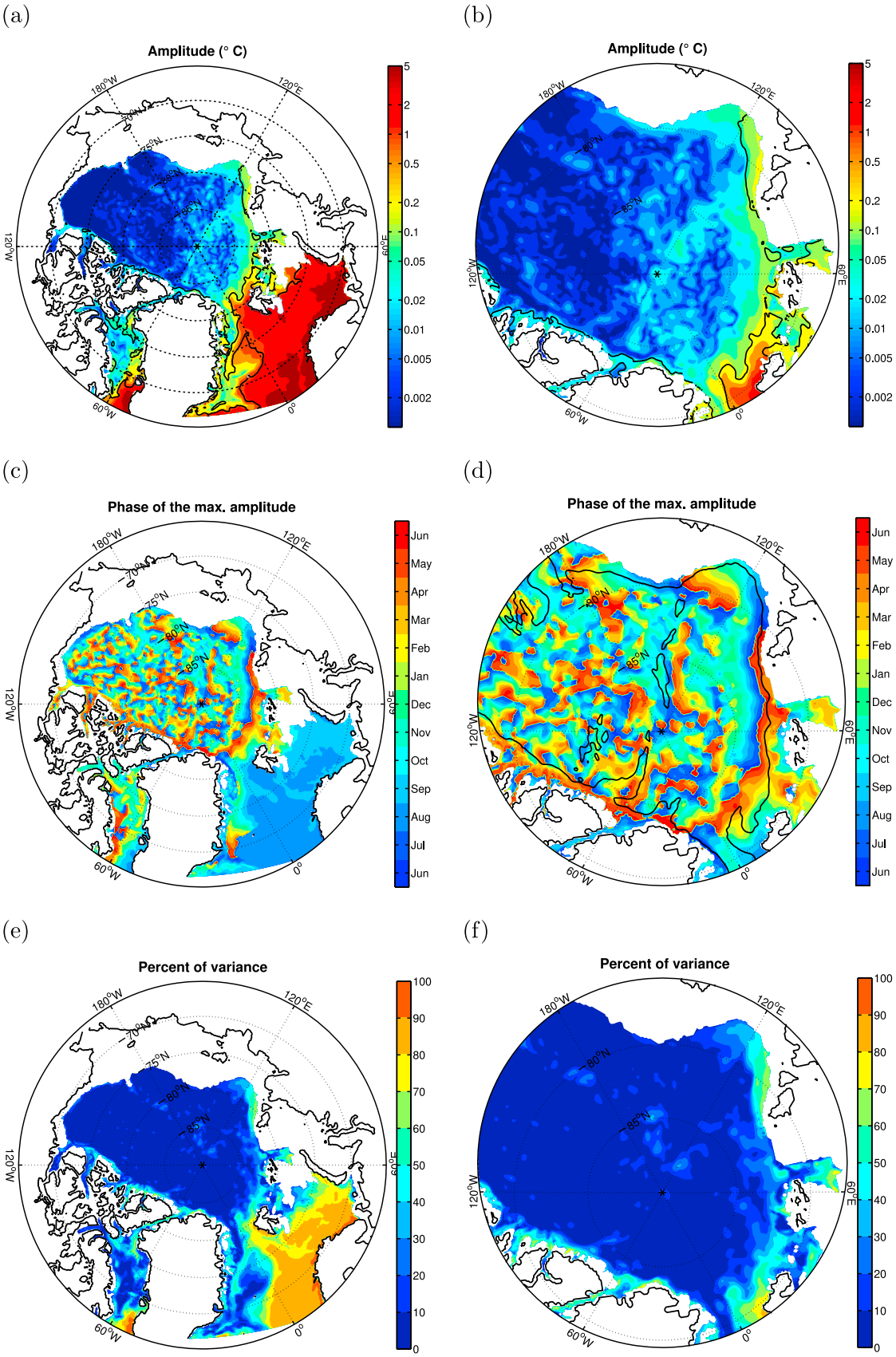
(a)
Amplitude (° C)
5
2
1
0.5
0.2
0.1
0.05
0.02
0.01
0.005
0.002
(b)
Amplitude (° C)
(c)
Phase of the max. amplitude
Jun
May
Apr
Mar
Feb
Jan
Dec
Nov
Oct
Sep
Aug
Jul
Jun
(d)
Phase of the max. amplitude
(e)
Percent of variance
100
90
80
70
60
50
40
30
20
10
0
(f)
Percent of variance
180°W
120°E
120°W
60°E
60°W
0°
70°N
75°N
80°N
85°N

Figure 8

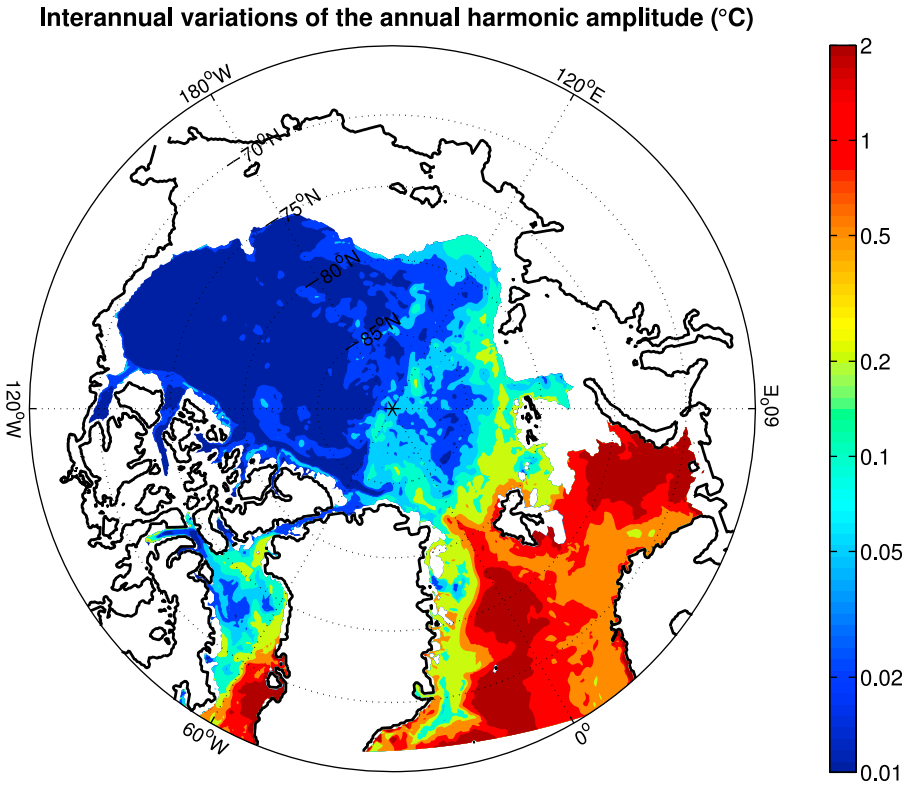

Figure 9. Interannual variations of the annual harmonic amplitude for the seasonal AWCT time series. At each grid point, the annual harmonic is computed for a running 5-year window. The range (i.e., the maximum minus the minimum amplitude) is then computed. Note that the color scale for the range is not linear.

variance explained by the annual harmonic. The 95% significance level of the annual harmonic fitting according to an F test is also indicated. In the North Atlantic sector up to the entrance of the Arctic Basin, the annual harmonic explains more than 70% of the total AWCT variance. The amplitude of the seasonal cycle is larger than 2°C, and the maximum occurs in August, when the net accumulated heat during summer has reached its maximum. The amplitude in the southern Barents Sea is around 2°C, which is consistent with the results of *Smedsrud et al.* [2010]. As AW descends under the ice cover, the amplitude of the annual harmonic and the percentage of variance explained by this harmonic decrease, and no coherent phase is found in the basin. Significant amplitude (around 0.1°C) and explained variance (around 40%) can be found along the Nansen Basin slope up to the Laptev Sea. On the slope, the phase of the AWCT seasonal maximum is changing along the AW pathway, from August in Fram Strait to May at the St. Anna Trough to October at the end of the Nansen Basin. This pattern suggests an advection process that delays the phase by the time taken by the travel of the water mass. This will be discussed in detail in the following section.

[27] The spatial pattern of the seasonal AWCT amplitude is similar to the mean AWCT (Figure 2). Large amplitude values (although not significant at the 95% level) are found in the Nansen Basin interior where the model mean AWCT is larger than 1°C. In contrast, the amplitude of the annual harmonic is negligible over the Makarov and Canada basins, where the seasonal variations of the AWCT accounts for a negligible part of the total variance. The correlation between the mean AWCT and the annual harmonic amplitude in the entire Arctic Basin is 0.75, suggesting that the loss of heat along the AW pathway by diffusion and mixing occurs concurrent with a weakening of the seasonal cycle strength.

4.3. Interannual Variations of Seasonal Cycle Amplitude

[28] The seasonal cycle amplitude varies largely interannually (Figure 7). For example, between 1990 and 1995, the peak-to-peak amplitude at M3 is about twice as large as the mean annual harmonic amplitude. The timing of the maximum and minimum may change from year to year by a few months (Figure 7), making it difficult to define the seasonal cycle amplitude and timing for a given year. In order to get an idea of the interannual variability of the AWCT seasonal cycle amplitude in the basin, we compute the range of the annual harmonic amplitude, as defined in Figure 9.

Figure 8. (a) Peak-to-peak amplitude, (c) phase of annual harmonic and (e) percent of the total variance explained by this harmonic for the seasonal AWCT time series. See Figure 7 for the treatment applied to the model AWCT. Note that the color scale for the amplitude is not linear, and that June is both represented by blue and red for the phase. (b, d, and f) Same as Figures 8a, 8c and 8e but focused on the Nansen Basin. The 95% significance level of the annual harmonic fitting according to a F-test is indicated on Figures 8a and 8b (black line). The 1500 m isobath is shown on Figure 8d (black line).

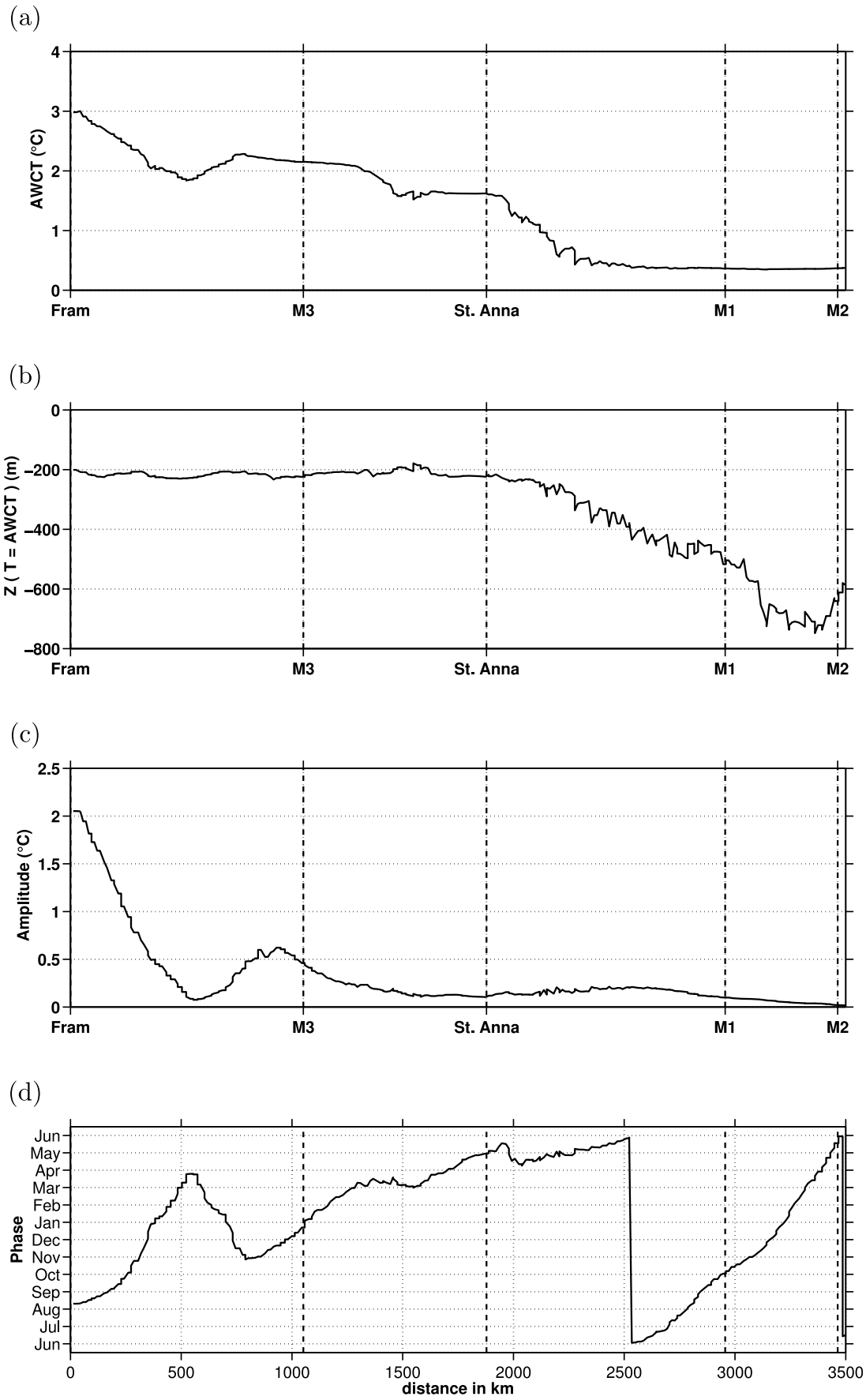
(a)
AWCT (°C)
4
3
2
1
0
Fram
M3
St. Anna
M1
M2
(b)
Z (T = AWCT) (m)
0
−200
−400
−600
−800
Fram
M3
St. Anna
M1
M2
(c)
Amplitude (°C)
2.5
2
1.5
1
0.5
0
Fram
M3
St. Anna
M1
M2
(d)
Phase
Jun
May
Apr
Mar
Feb
Jan
Dec
Nov
Oct
Sep
Aug
Jul
Jun
0
500
1000
1500
2000
2500
3000
3500
distance in km

Figure 10

[29] Looking at the region where the annual harmonic fit is significant (in the North Atlantic sector and along the Nansen basin slope, see Figure 8b), we find that the interannual variations of the seasonal cycle amplitude can be almost as large as the seasonal cycle amplitude. This variability makes it even more difficult to characterize the seasonal cycle at a given point from a mooring, as it only samples a short time period. For instance, the seasonal cycle amplitude at M1 and M2 described by *Dmitrenko et al.* [2006, 2009], respectively, could have been different both in terms of amplitude and phase if sampled during a different period. According to the model, the interannual variations of the AWCT annual harmonic amplitude at M1 and M2 are 0.11°C and 0.05°C, respectively, while the annual harmonic amplitudes are 0.03°C and 0.01°C at these locations.

5. Nansen Basin Processes

[30] The AWCT exhibits a significant seasonality only in the Nansen Basin along the AW pathway following the slope from Fram Strait to the Laptev Sea (Figure 8). To explain the seasonality in this region, we examine the mean and the variations of the AWCT along the 1500 m isobath from Fram Strait to the Laptev Sea (see Figure 3 for the location of the isobath). This isobath is a reasonable choice to follow the pathway of the AW [*Schauer et al.*, 1997]. Figure 10 shows the mean AWCT and the depth of the AWCT, as well as the annual amplitude and phase (as shown in Figure 8) along the 1500 m isobath. Figure 11 shows the time-distance diagrams of the AWCT, the seasonal AWCT (as defined in the previous section) and the velocity amplitude at the depth of the AWCT. The power spectrum density of the AWCT and the velocity amplitude are computed at each point along the isobath from the monthly means values over the period 1980–2007, and the results are shown in Figure 12.

[31] Along the Nansen Basin slope, the mean AWCT decreases from 3°C to about 0.4°C at M2 (Figure 10a). The alternation between multiyear cold and warm events is clearly visible from Figure 11a, which is in agreement with the model results of *Karcher et al.* [2003] and the observations northwest of Svalbard of *Saloranta and Haugan* [2001], who describe the spreading of two warm events in the 1980s and 1990s. Although this low-frequency variability of AW temperature is dominant in the Arctic Basin downstream from Fram Strait and the Barents Sea, Figure 12 also reveals the existence of a seasonality for the AWCT and its associated velocity along the 1500 m isobath. This seasonality and the large spatial variations of the velocity along the slope mean that we can not just transform space into time in order to examine the propagation of the seasonal cycle, as has been done for instance by *Timofeyev* [1962] to determine the transit time of AW within the Nansen Basin. In what follows, we will examine step by step this seasonality from Fram Strait to the Laptev Sea.

[32] The AWCT at Fram Strait exhibits a large seasonal cycle amplitude (more than 2°C), with a maximum at the surface during summer and a minimum during winter deeper (around 200 to 400 m), due to local winter convection [*Haugan*, 1999]. From Fram Strait to M3, the model simulated AW core splits up into two branches (not shown): one follows the 1500 m isobath and then mostly recirculates to Fram Strait, while the second branch flows over the Yermak plateau. This is consistent with the circulation sketch proposed by *Bourke et al.* [1988] and confirmed by *Walczowski and Piechura* [2007]. As a consequence, much of the AW core that enters the Arctic Ocean follows the shortcut over the Yermak plateau, which explains the fast and large decrease and then increase of the AWCT and its seasonal cycle amplitude (Figure 10). Around 800 km, the main AW core again reaches the 1500 m isobath.

[33] Close to M3, the AWCT exhibits a seasonal cycle amplitude of about 0.5°C, with the maximum found at a constant depth between 200 and 300 m, except in 1990 and between 1999 and 2001, when the AWCT is deeper in winter (∼500 m). These events correspond to episodes when the Barents Sea was completely free of ice in the model (also visible in NSIDC sea ice extent observations [*Fetterer et al.*, 2002]), leading to local convection due to a large release of heat to the atmosphere. At mooring M3, the maximum of the annual harmonic occurs in January, i.e., 5 months later than in Fram Strait. This is consistent with an advection of the AW seasonal cycle along slope, as suggested by *Ivanov et al.* [2009].

[34] Near St. Anna Trough, the amplitude of the annual harmonic decreases to 0.1°C, while the timing of the maximum occurs later in the year, consistent again with an advection process of the seasonal cycle. On top of that, Figures 11 and 12 show that the timing of the seasonal cycle becomes more and more irregular as AW penetrates further downstream in the Arctic Basin and the cold and warm seasons becomes difficult to distinguish just before the St. Anna Trough.

[35] Less saline and colder AW modified in the Barents Sea penetrates into the Arctic Ocean through St. Anna Trough. This branch of AW undergoes vigorous mixing with the Fram Strait branch of AW while spreading eastward following the slope of the Nansen Basin [*Schauer et al.*, 1997]. This results in a large decrease of the AWCT and its depth after St. Anna Trough (Figures 10a, 10b and 11a). In the model, the seasonal maximum AWCT for the Barents Sea Branch just upstream from St. Anna Trough occurs in winter (February–March, not shown), i.e., just a few months earlier in the year than the maximum of the Fram Strait Branch at that location (April–May, Figure 10d), which makes the interference between the two branches nearly constructive. The phase of the seasonal cycle of the Barents Sea Branch results from interplay between several processes, including advection of AW from the entrance of the Barents Sea to the St. Anna Trough (that takes only around one year in the model [*Lique et al.*, 2010], which might be too fast compared to observed velocities in the Barents Sea [*Årthun et al.*, 2011]), mixing that leads to strong cooling [*Schauer et al.*, 2002a] and seasonal and year-to-year variations of

Figure 10. Evolution along the 1500 m isobath of (a) the mean AWCT averaged over 1980–2007, (b) the mean depth of the AWCT and the AWCT annual harmonic (c) amplitude and (d) phase. The 0-contour is shown on Figure 10b (white line). The distance starts at Fram Strait. The black dotted lines marks (from left to right) the locations of mooring M3, St. Anna Trough, and moorings M1 and M2. See Figure 3 for the location of the isobath.

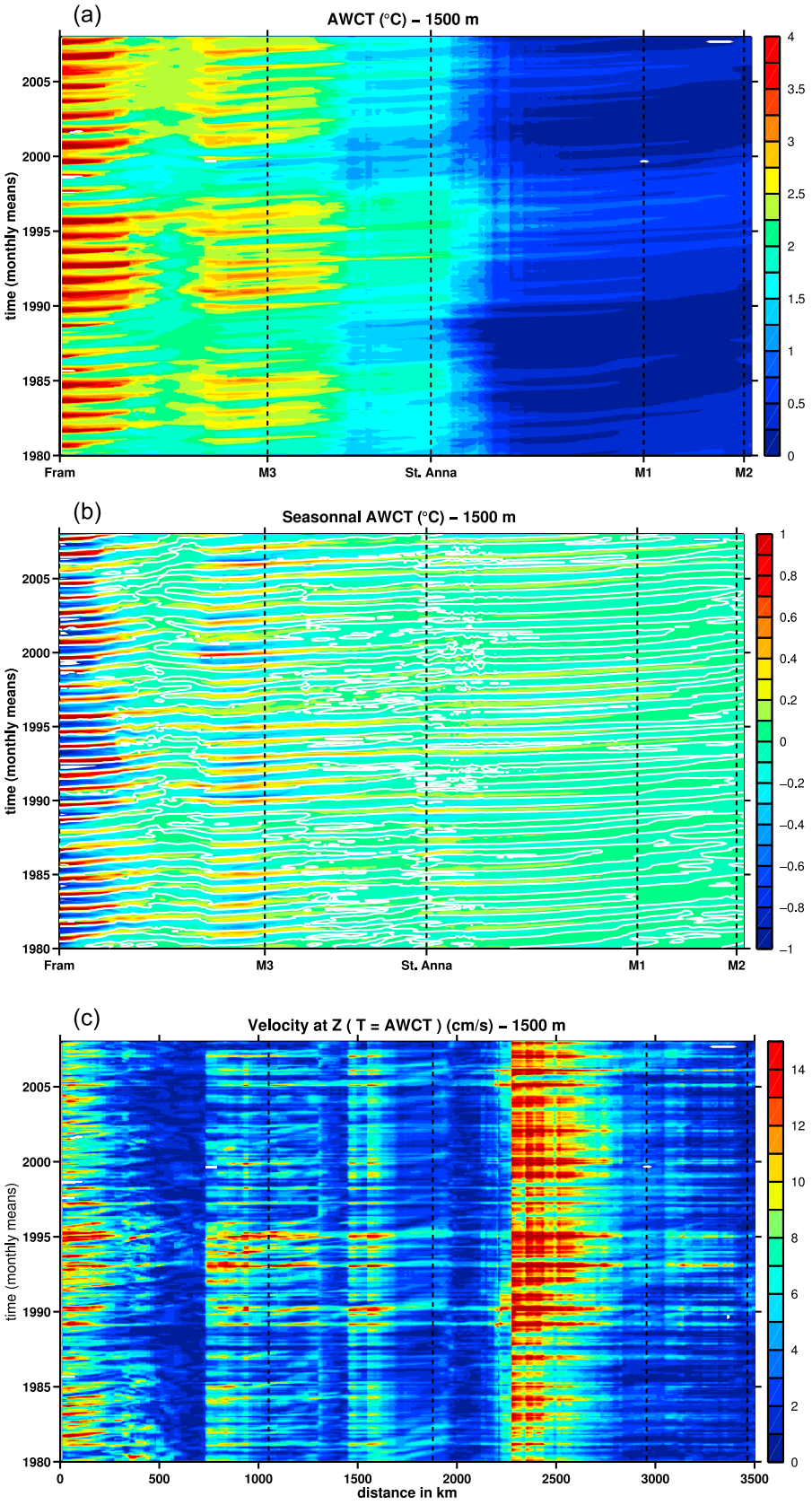

Figure 11. Time-distance diagrams along (a) the 1500 m isobath of the AWCT, (b) the seasonal AWCT (see Figure 7 for the definition of this quantity) and (c) the velocity amplitude found at the depth of the AWCT. The distance starts at Fram Strait. The black dotted lines marks (from left to right) the locations of mooring M3, St. Anna Trough, and moorings M1 and M2. See Figure 3 for the location of the isobath.

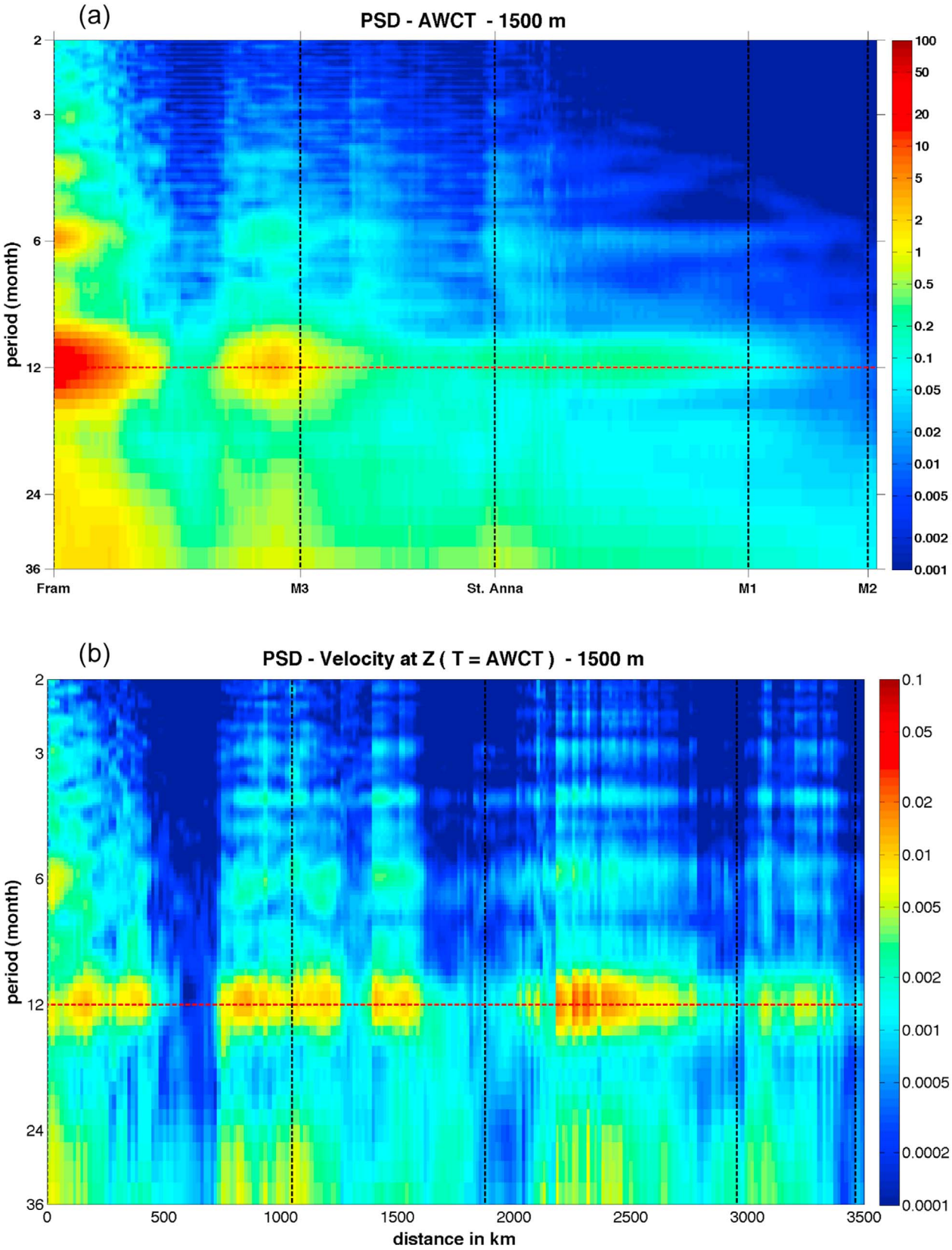

Figure 12. Power spectrum density (PSD) of (a) the AWCT (in $°C^2$/cycle per month) and (b) the velocity at Z(T = AWCT) (in $(m/s)^2$/cycle per month) along the 1500 m isobath. The distance starts at Fram Strait. The black dotted lines marks (from left to right) the locations of mooring M3, St. Anna Trough, and moorings M1 and M2. See Figure 3 for the location of the isobath.

the sea ice edge location [*Aksenov et al.*, 2010]. Although of importance, the understanding of the AW seasonal cycle timing in the Barents Sea is beyond the scope of this paper.

[36] Along the Nansen slope, as the Fram Strait and the Barents Sea branches mix, the AWCT decreases while the amplitude of the annual harmonic (Figure 10c) and the energy around the 12-month frequency (Figure 12a) increase slightly. The month of the annual harmonic maximum first decreases from May to April around 2000 km, and then increases again in a consistent way with a propagation responsible for the seasonal cycle. The timing of the seasonal cycle appears to be more regular (Figure 11b) after the decrease of the AWCT east of St. Anna Trough (Figure 11a). The depth associated with the maximum also increases after this point (Figure 10b). These changes indicate that the propagating Fram Strait seasonal signal is re-energized by new input from the Barents Sea Branch. As it continues further downstream, the seasonal amplitude gradually decreases, and the timing of the cycle becomes less regular (Figure 11b), as confirmed by a decrease in the power spectrum density at seasonal time scale (Figure 12). In the Laptev Sea at moorings M1 and M2, the annual harmonic is not significant anymore; the separation between a cold and a warm season can only be made in some years (Figure 11b). The timing and the amplitude of the seasonal cycle are strongly year dependent.

[37] Observations from M1 suggest that the seasonal cycle there could be due to a shift of the AW core toward the slope in winter and away in summer [*Dmitrenko et al.*, 2006]. In order to test this hypothesis, we consider the seasonal cycle of the AWCT along different isobaths (between 1000 m and 2500 m, not shown). The AWCT seasonal cycle appears to be in phase at a given distance from Fram Strait along both deeper and shallower isobaths, and there is no shift of the AW core between different isobaths.

[38] The velocity of the AWCT exhibits a large seasonal cycle (Figure 12b), that is in phase all along the isobath (Figure 11c), possibly due to a basin scale coherent mode of the circulation. This suggests that the AWCT is advected along the slope at a velocity that varies seasonally and spatially along the slope, but not spatially across the slope. How does the variability of AW velocity affect the decline in its seasonal cycle amplitude eastward along the Nansen Basin slope? We consider three scenarios. First, imagine a scenario with uniform velocity in the presence of diffusion and eddy generation by flow instability. In this case, warm and cold season signatures will propagate along this pathway at the same speed. The amplitude of the seasonal difference between these signatures at a particular location will decrease downstream, since diffusion is proportional to spatial temperature gradients and thus will cool the warm season signal faster than the cold season signal. Eddies may also be generated along the pathway which will cool the AW and affect the seasonal amplitude in an unknown and possibly random manner. Second, consider a case wherein the velocity is uniform in space, but varies seasonally. Here again the warm and cold season signatures propagate at the same speed, although this speed changes over the year. Thus diffusion will reduce the seasonal amplitude, while eddies will preferentially cool the current during the fast season (when instability is more likely) but may not affect the seasonal amplitude per se. Finally, consider the result of our model simulation (Figure 11c): a (nearly) fixed spatial pattern of velocity along the Nansen Basin slope with seasonally varying amplitude. In this case, diffusion is enhanced by flux convergence along the pathway. For example, deceleration of the current along its pathway will reduce the distance between warm and cold season signatures, encouraging mixing between them which reduces the seasonal amplitude and makes its timing less regular. The interplay between velocity and temperature variations along the AW pathway is clearly an interesting and complex subject that, while beyond the scope of the present study, merits further analysis.

6. Summary and Discussion

[39] The AW in the Arctic Ocean lies at intermediate depth and thus does not have direct contact with the atmosphere, yet its temperature exhibits a seasonal cycle in parts of the basin. The amplitude of the seasonal cycle is strongly space dependent, and in the model simulation, significant values are only found in the Nansen Basin along the slope where the AW is primarily advected [*Schauer et al.*, 2004], while no significant seasonality of the AW temperature could be found in the in the Canada and Makarov Basins. From Fram Strait to the Laptev Sea, the phase of the AWCT annual harmonic is gradually delayed, which is consistent with an advection process. The delay is about one year over the 2000 km that separates the Laptev Sea from Fram Strait (Figure 10). Assuming a constant advection, this would require a velocity of 6 cm/s. This is consistent with the velocities observed through Fram Strait [*Schauer et al.*, 2004], with those observed at mooring M3 [*Ivanov et al.*, 2009], with the advection speed (∼8 cm/s) estimated along the Eurasian continental slope by *Swift et al.* [1997], and with the speed calculated by *Woodgate et al.* [2001] (∼5 cm/s) between St. Anna Through and M1. On the other hand, our model's propagation speed appears to be faster than the estimate of *Polyakov et al.* [2005], who suggest that the warm event observed at the mooring M1 in 2004 has taken 5 years to propagate from Fram Strait, which corresponds to a mean velocity of 1.5 cm/s, or the estimate of *Frank et al.* [1998], who deduce mean current speed of about 1 cm/s using tracer measurements in the Eurasian Basin. Although our model advection speed appears faster than some available estimates in the literature, the sparseness of velocity observations along the Nansen slope, as well as the large variability of the velocities along and across the slope makes it difficult to assess the realism of our model simulated velocities.

[40] Moreover, model simulated AWCT and velocity exhibit a seasonal cycle with different phase along the Eurasian slope; the velocity of the AW layer has a seasonal cycle that is in phase around the Nansen Basin. Investigation into the origin of the velocity coherent seasonal cycle is beyond the scope of this paper. Our results suggest that the AWCT seasonal cycle can survive over a long but finite distance (around 1000 km). From Fram Strait to St. Anna Trough, the temperature seasonal cycle originates from the Fram Strait Branch, while after St. Anna Trough the temperature seasonal cycle is dominated by the Barents Sea Branch. We speculate that mixing and diffusion processes as well as the spatial variations of the velocity (that might also enhance the mixing) along the AW advection path leads to the gradual disappearance of the AWCT seasonality. As in

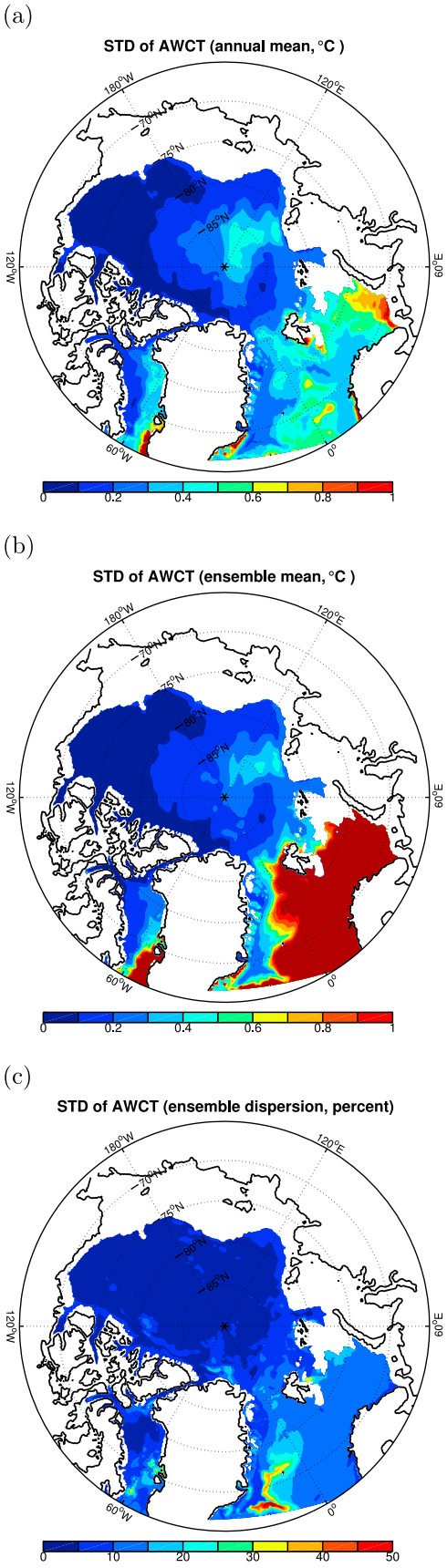

most non-eddy resolving models, diffusion is here probably overly strong, which could explain our AW cold bias and might also cause an underestimation of AWCT seasonality.

[41] In addition to the large spatial variations, the amplitude of the AWCT seasonal cycle also largely varies from year to year, and its variations can be almost as large as the mean amplitude (Figure 9). This suggests that it might be difficult to characterize this quantity from observations spanning only one or two years.

[42] Due to environmental conditions, in situ non-autonomous measurements are conducted in the Arctic Ocean mostly during spring (aircraft-based observations) and late summer (ship-based observations); only a sub-sample of the seasonal cycle is measured. One could logically infer that this seasonal bias of the observations might lead to large uncertainty (at least in some regions) when examining interannual variations or long term trends of AW properties. In order to get insight on the possible impact of this subsampling, we subsample our AWCT time series by randomly choosing a month each year. The same calculation is reproduced 1000 times using different randomly chosen months in order to obtain an ensemble for which we then compute the mean standard deviation over 1980–2007 of the AWCT and the dispersion (i.e., the standard deviation of the ensemble) around this mean standard deviation. The mean standard deviation is compared to the standard deviation over 1980–2007 of the AWCT computed from annual means. Results are shown in Figure 13. Large discrepancies are visible in regions free of ice or seasonally ice-covered. In contrast, in the Arctic Ocean where AW lies under the cold mixed layer and halocline, standard deviations computed from annual or randomly chosen monthly means are in near agreement, and the dispersion of the ensemble is less than 10%. Note that our computation represents the worst case scenario, as in reality, almost all the measurements are conducted during spring and summer, which would reduce the dispersion of the ensemble. This suggests that the error induced by seasonal sampling bias when computing long term variability [e.g., *Polyakov et al.*, 2004] is small, even in the regions where the seasonal cycle amplitude is significant.

[43] Figure 14 shows the ratio between the amplitude of the AWCT seasonal cycle and the variations of the AWCT annual mean. This shows that in the Arctic Ocean, the AWCT seasonal variations are small compared to the amplitude of the interannual variations, while in the ice-free areas to the south, the seasonal variations are dominant. We thus suggest that seasonally biased measurements of the AW temperature are sufficient to examine its interannual variations. The only exception might be the region northeast of Fram Strait, where the annual harmonic amplitude is larger than the standard deviation of AWCT computed from the annual mean. Long-term mooring data such as at M3 deployed in this region might help to develop a correction

Figure 13. (a) Standard deviation of the AWCT computed from annual mean. (b) Mean and (c) dispersion (defined as the standard deviation of the ensemble) of the standard deviation of the AWCT computed from randomly chosen monthly mean. The ensemble consists of 1000 realizations. The linear trend has been removed from the time series to compute the standard deviation.

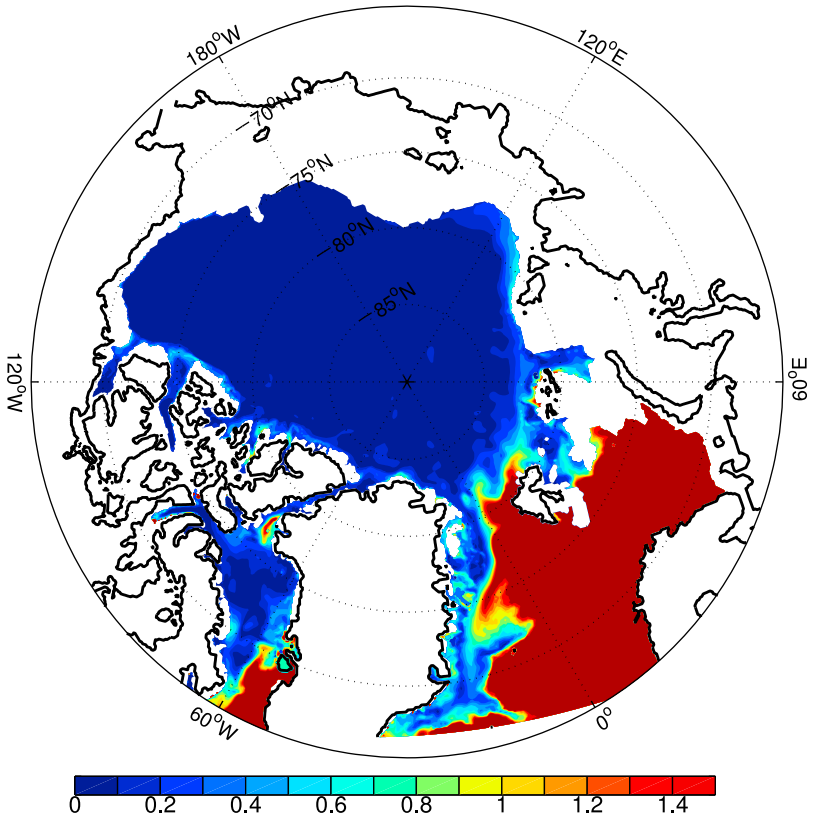

Figure 14. Amplitude of the AWCT annual harmonic divided by two standard deviations from annual mean of the AWCT time series. This compares the part of the AWCT variability due to the seasonal cycle and the part due to interannual variations. The linear trend of the time series has been removed to compute the standard deviation.

for the seasonally sub-sampled measurements conducted in this region.

[44] **Acknowledgments.** We sincerely thank all the people who provided the observations used in this study, namely Andrey Proshutinsky (BGOS), Igor Polyakov (NABOS), Knut Aagaard and James Morison (NPEO), Vladimir Ozhigin (Kola section), and Agnieszka Beszczynska (Fram Strait). This study uses numerical experiments carried out within the European DRAKKAR project. The simulation has been run at the IDRIS CNRS-GENCI computer centre in Orsay, France, by J. M. Molines. We thank Knut Aagaard, Cecilia Ferriz and Anne Marie Treguier for helpful comments and suggestions on an earlier version of the manuscript. Lars Smedsrud, Tore Furevik and Andrey Proshutinsky provided valuable comments. We also thank Harry Stern and Rebecca Woodgate for advice on statistical analysis. C. Lique is supported by JISAO and the Program for Climate Change of the University of Washington. M. Steele is supported by NSF's office of polar programs and NASA's cryosphere and biogeosciences programs.

References

Aagaard, K., R. Andersen, J. Swift, and J. Johnson (2008), A large eddy in the central Arctic Ocean, *Geophys. Res. Lett.*, *35*, L09601, doi:10.1029/2008GL033461.

Årthun, M., R. B. Ingvaldsen, L. H. Smedsrud, and C. Schrum (2011), Dense water formation and circulation in the Barents Sea, *Deep Sea Res. Part I*, *58*, 801–817, doi:10.1016/j.dsr.2011.06.001.

Aksenov, Y., S. Bacon, A. C. Coward, and A. J. G. Nurser (2010), The North Atlantic inflow to the Arctic Ocean: High-resolution model study, *J. Mar. Syst.*, *79*, 1–22.

Aksenov, Y., V. V. Ivanov, A. J. G. Nurser, S. Bacon, I. V. Polyakov, A. C. Coward, A. C. Naveira-Garabato, and A. Beszczynska-Moeller (2011), The Arctic Circumpolar Boundary Current, *J. Geophys. Res.*, *116*, C09017, doi:10.1029/2010JC006637.

Barnier, B., et al. (2006), Impact of partial steps and momentum advection schemes in a global ocean circulation model at eddy permitting resolution, *Ocean Dyn.*, *56*, 543–567, doi:10.1007/s10236-006-0082-1.

Bourke, R. H., A. M. Weigel, and R. G. Paquette (1988), The westward turning branch of the West Spitsbergen Current, *J. Geophys. Res.*, *931*, 14,065–14,077, doi:10.1029/JC093iC11p14065.

Brodeau, L., B. Barnier, T. Penduff, A. M. Treguier, and S. Gulev (2010), An ERA40-based atmospheric forcing for global ocean circulation models, *Ocean Modell.*, *31*, 88–104.

Carmack, E. C., K. Aagaard, J. H. Swift, R. W. MacDonald, F. A. McLaughlin, E. Peter Jones, R. G. Perkin, J. N. Smith, K. M. Ellis, and L. R. Killius (1997), Changes in temperature and tracer distributions within the Arctic Ocean: Results from the 1994 Arctic Ocean section, *Deep Sea Res. Part II*, *44*, 1487–1502, doi:10.1016/S0967-0645(97)00056-8.

Coachman, L. K., and C. A. Barnes (1963), The movement of Atlantic Water in the Arctic Ocean, *J. Arct. Inst. N. Am.*, *16*, 8–16.

Dai, A., and K. Trenberth (2002), Estimates of freshwater discharge from continents: Latitudinal and seasonal variations, *J. Hydrometeorol.*, *3*, 660–687.

Dmitrenko, I. A., I. V. Polyakov, S. A. Kirillov, L. A. Timokhov, H. L. Simmons, V. V. Ivanov, and D. Walsh (2006), Seasonal variability of Atlantic water on the continental slope of the Laptev Sea during 2002–2004, *Earth Planet. Sci. Lett.*, *244*, 735–743.

Dmitrenko, I. A., I. V. Polyakov, S. A. Kirillov, L. A. Timokhov, I. E. Frolov, V. T. Sokolov, H. L. Simmons, V. V. Ivanov, and D. Walsh (2008), Toward a warmer Arctic Ocean: Spreading of the early 21st century Atlantic Water warm anomaly along the Eurasian Basin margins, *J. Geophys. Res.*, *113*, C05023, doi:10.1029/2007JC004158.

Dmitrenko, I. A., et al. (2009), Seasonal modification of the Arctic Ocean intermediate water layer off the eastern Laptev Sea continental shelf break, *J. Geophys. Res.*, *114*, C06010, doi:10.1029/2008JC005229.

Fetterer, F., K. Knowles, W. Meier, and M. Savoie (2002), Sea ice index, http://nsidc.org/data/seaice_index/, Natl. Snow and Ice Data Cent., Boulder, Colo. [Updated 2009.]

Frank, M., W. M. Smethie, and R. Bayer (1998), Investigation of subsurface water flow along the continental margin of the Eurasian Basin using the transient tracers tritium, ^{3}He, and CFCs, *J. Geophys. Res.*, *103*(C13), 30,773–30,792, doi:10.1029/1998JC900003.

Furevik, T. (2001), Annual and interannual variability of Atlantic Water temperatures in the Norwegian and Barents Seas: 1980–1996, *Deep Sea Res. Part I*, *48*, 383–404, doi:10.1016/S0967-0637(00)00050-9.

Haugan, P. M. (1999), Structure and heat content of the West Spitsbergen Current, *Natl. Inst. Polar Res. Mem.*, *18*, 183–188, doi:10.1111/j.1751-8369.1999.tb00291.x.

Hunke, E., M. Maltrud, and M. Hecht (2008), On the grid dependence of lateral mixing parameterizations for global ocean simulations, *Ocean Modell.*, *20*, 115–133, doi:10.1016/j.ocemod.2007.06.010.

Ivanov, V., I. Polyakov, I. Dmitrenko, E. Hansen, I. Repina, S. Kirillov, C. Mauritzen, H. Simmons, and L. Timokhov (2009), Seasonal variability in Atlantic Water off Spitsbergen, *Deep Sea Res. Part I*, *56*, 1–14.

Karcher, M. J., and J. M. Oberhuber (2002), Pathways and modification of the upper and intermediate waters of the Arctic Ocean, *J. Geophys. Res.*, *107*(C6), 3049, doi:10.1029/2000JC000530.

Karcher, M. J., R. Gerdes, F. Kauker, and C. Köberle (2003), Arctic warming: Evolution and spreading of the 1990s warm event in the Nordic seas and the Arctic Ocean, *J. Geophys. Res.*, *108*(C2), 3034, doi:10.1029/2001JC001265.

Large, W., and S. Yeager (2004), Diurnal to decadal global forcing for ocean and sea-ice models: The datasets and flux climatologies, *Tech. Note NCAR/TN-460+STR*, Natl. Cent. for Atmos. Res., Boulder, Colo.

Lengaigne, M., G. Madec, L. Bopp, C. Menkes, O. Aumont, and P. Cadule (2009), Bio-physical feedbacks in the Arctic Ocean using an Earth system model, *Geophys. Res. Lett.*, *36*, L21602, doi:10.1029/2009GL040145.

Lique, C., A. M. Treguier, M. Scheinert, and T. Penduff (2009), A model-based study of ice and freshwater transport variability along both sides of Greenland, *Clim. Dyn.*, *33*, 685–705, doi:10.1007/s00382-008-0510-7.

Lique, C., A. M. Treguier, B. Blanke, and N. Grima (2010), On the origins of water masses exported along both sides of Greenland: A Lagrangian model analysis, *J. Geophys. Res.*, *115*, C05019, doi:10.1029/2009JC005316.

Loeng, H. (1991), Features of the physical oceanographic conditions of the Barents Sea, *Natl. Inst. Polar Res. Mem.*, *10*, 5–18, doi:10.1111/j.1751-8369.1991.tb00630.x.

Madec, G. (2008), NEMO ocean engine, *Note Pôle Modél. 27*, Inst. Pierre-Simon Laplace, Paris.

McLaughlin, F. A., E. C. Carmack, W. J. Williams, S. Zimmermann, K. Shimada, and M. Itoh (2009), Joint effects of boundary currents and thermohaline intrusions on the warming of Atlantic water in the Canada Basin, 1993–2007, *J. Geophys. Res.*, *114*, C00A12, doi:10.1029/2008JC005001.

Morison, J., et al. (2002), North Pole Environmental Observatory delivers early results, *Eos Trans. AGU*, *83*(33), 357,360–361.

Nøst, O. A., and P. E. Isachsen (2003), The large-scale time-mean ocean circulation in the Nordic Seas and Arctic Ocean estimated from simplified dynamics, *J. Mar. Res.*, *61*, 175–210.

Penduff, T., J. Le Sommer, B. Barnier, A.-M. Treguier, J.-M. Molines, and G. Madec (2007), Influence of numerical schemes on current-topography interactions in 1/4 global ocean simulations, *Ocean Sci.*, *3*, 509–524.

Pickart, R. S., M. A. Spall, G. W. K. Moore, T. J. Weingartner, R. A. Woodgate, K. Aagaard, and K. Shimada (2011), Upwelling in the Alaskan Beaufort Sea: Atmospheric forcing and local versus non-local response, *Prog. Oceanogr.*, *88*, 78–100.

Polyakov, I., D. Walsh, I. Dmitrenko, R. Colony, J. Hutchings, L. Timokhov, M. Johnson, and E. Carmack (2003), A long-term circulation and water mass monitoring program for the Arctic Ocean, *Eos Trans. AGU*, *84*(30), 281,284–285.

Polyakov, I. V., G. V. Alekseev, L. A. Timokhov, U. S. Bhatt, R. L. Colony, H. L. Simmons, D. Walsh, J. E. Walsh, and V. F. Zakharov (2004), Variability of the Intermediate Atlantic Water of the Arctic Ocean over the last 100 years, *J. Clim.*, *17*, 4485–4497.

Polyakov, I. V., et al. (2005), One more step toward a warmer Arctic, *Geophys. Res. Lett.*, *32*, L17605, doi:10.1029/2005GL023740.

Proshutinsky, A., R. Krishfield, M.-L. Timmermans, J. Toole, E. Carmack, F. McLaughlin, W. J. Williams, S. Zimmermann, M. Itoh, and K. Shimada (2009), Beaufort Gyre freshwater reservoir: State and variability from observations, *J. Geophys. Res.*, *114*, C00A10, doi:10.1029/2008JC005104.

Quadfasel, D., A. Sy, D. Wells, and A. Tunik (1991), Warming in the Arctic, *Nature*, *350*, 385, doi:10.1038/350385a0.

Rudels, B., E. P. Jones, L. G. Anderson, and G. Kattner (1994), On the intermediate depth waters of the Arctic Ocean, in *The Polar Oceans and Their Role in Shaping the Global Environment*, *Geophys. Monogr. Ser.*, vol. 85, edited by O. M. Johannessen, R. Muench, and J. Overland, pp. 33–46, AGU, Washington, D. C.

Rudels, B., H. Jfriedrich, and D. Quadfasel (1999), The Arctic Circumpolar Boundary Current, *Deep Sea Res. Part II*, *46*, 1023–1062, doi:10.1016/S0967-0645(99)00015-6.

Saloranta, T. M., and P. M. Haugan (2001), Interannual variability in the hydrography of Atlantic water northwest of Svalbard, *J. Geophys. Res.*, *106*, 13,931–13,944, doi:10.1029/2000JC000478.

Schauer, U., R. D. Muench, B. Rudels, and L. Timokhov (1997), Impact of eastern Arctic shelf waters on the Nansen Basin intermediate layers, *J. Geophys. Res.*, *102*, 3371–3382, doi:10.1029/96JC03366.

Schauer, U., H. Loeng, B. Rudels, V. K. Ozhigin, and W. Dieck (2002a), Atlantic Water flow through the Barents and Kara seas, *Deep Sea Res. Part I*, *49*, 2281–2298.

Schauer, U., B. Rudels, E. P. Jones, L. G. Anderson, R. D. Muench, G. Björk, J. H. Swift, V. Ivanov, and A.-M. Larsson (2002b), Confluence and redistribution of Atlantic water in the Nansen, Amundsen and Makarov basins, *Ann. Geophys.*, *20*, 257–273.

Schauer, U., E. Fahrbach, S. Osterhus, and G. Rohardt (2004), Arctic warming through the Fram Strait: Oceanic heat transport from 3 years of measurements, *J. Geophys. Res.*, *109*, C06026, doi:10.1029/2003JC001823.

Smedsrud, L. H., R. Ingvaldsen, J. E. Ø. Nilsen, and Ø. Skagseth (2010), Heat in the Barents Sea: Transport, storage, and surface fluxes, *Ocean Sci.*, *6*, 219–234.

Smolyar, I., and N. Adrov (2003), The quantitative definition of the Barents Sea Atlantic Water: Mapping of the annual climatic cycle and interannual variability, *ICES J. Mar. Sci.*, *60*, 836–845.

Steele, M., R. Morley, and W. Ermold (2001), PHC: A global ocean hydrography with a high quality Arctic Ocean, *J. Clim.*, *14*, 2079–2087.

Swift, J. H., E. P. Jones, K. Aagaard, E. C. Carmack, M. Hingston, R. W. MacDonald, F. A. McLaughlin, and R. G. Perkin (1997), Waters of the Makarov and Canada basins, *Deep Sea Res. Part II*, *44*, 1503–1529, doi:10.1016/S0967-0645(97)00055-6.

The DRAKKAR Group (2007), Eddy-permitting ocean circulation hindcasts of past decades, *CLIVAR Exch.*, *12*(3), 8–10.

Timmermann, R., H. Goosse, G. Madec, T. Fichefet, C. Ethe, and V. Duliere (2005), On the representation of high latitude processes in the ORCA-LIM global coupled sea ice-ocean model, *Ocean Modell.*, *8*, 175–201.

Timofeyev, V. T. (1962), The movement of Atlantic water and heat into the Arctic Basin [translated from Russian], *Okeanologiya*, *1*(3), 407–411.

Walczowski, W., and J. Piechura (2007), Pathways of the Greenland Sea warming, *Geophys. Res. Lett.*, *34*, L10608, doi:10.1029/2007GL029974.

Woodgate, R., K. Aagaard, R. Muench, J. Gunn, G. Bjork, B. Rudels, A. Roach, and U. Schauer (2001), The Arctic Ocean Boundary Current along the Eurasian slope and the adjacent Lomonosov Ridge: Water mass properties, transports and transformations from moored instruments, *Deep Sea Res. Part I*, *48*, 1757–1792, doi:10.1016/S0967-0637(00)00091-1.

Yashayaev, I. M., and I. I. Zveryaev (2001), Climate of the seasonal cycle in the North Pacific and the North Atlantic oceans, *Int. J. Climatol.*, *21*, 401–417, doi:10.1002/joc.585.

C. Lique, Joint Institute for the Study of the Atmosphere and Ocean, University of Washington, Box 355672, 3737 Brooklyn Ave. NE, Seattle, WA 98195–5672, USA. (liquec@uw.edu)

M. Steele, Polar Science Center, Applied Physics Laboratory, University of Washington, 1013 NE 40th St., Seattle, WA 98105, USA.